EGG-M--92378

DE92 017847

Particle-Fluid Two-Phase Flow Modeling[*]

Glen A. Mortensen[a] and John A. Trapp[b]

[a] *Idaho National Engineering Laboratory, EG&G Idaho, Inc., Idaho Falls, ID*

[b] *University of Colorado at Denver, CO, and Idaho National Engineering Laboratory, Idaho Falls, ID*

This paper describes a numerical scheme and computer program, DISCON, for the calculation of two-phase flows that does not require the use of flow regime maps. This model is intermediate between the local instantaneous and the averaged two-fluid model. It solves the Eulerian continuity, momentum, and energy equations for each liquid control volume, and the Lagrangian mass, momentum, energy, and position equations for each bubble. The bubbles are modeled individually using a large representative number of bubbles thus avoiding the numerical diffusion associated with Eulerian models. DISCON has been used to calculate the bubbling of air through a column of water and the subcooled boiling of water in a flow channel. The results of these calculations are presented.

1. INTRODUCTION

There are complex and challenging problems in the modeling and numerical simulation of two-phase flow. The Navier-Stokes equations with internal interfaces are intractable in all but the simplest cases. The averaged two-fluid model is the present state-of-the-art in two-phase flow. This paper describes a model that is intermediate between the Navier-Stokes description and the averaged two-fluid model. The dispersed phases are modeled using a Lagrangian description, and the continuous phases are modeled using an Eulerian description. This approach: (a) models the statistical features of the dispersed phase, (b) models the flow regime transitions, and (c) eliminates the numerical diffusion associated with purely Eulerian descriptions. Similar models have been used to model fuel sprays [1, 2, 3, and 4]. The extension of these models to two-phase flow presents an additional challenge because the volume occupied by the dispersed phase is no longer small compared to the computational cell size. JAYCOR has developed a similar model for bubbles in a continuous liquid phase [5] in which they addressed many of these additional challenges. However, the JAYCOR model did not solve the time-dependent mass, momentum, and energy equations for the continuous liquid phase, but used instead quasi-steady-state equations.

A computer code, DISCON, was written to implement this model. The model describes the motion of a dispersed phase using a Lagrangian description. The main motivation is to be able to predict flow regime transitions and represent a spectra of bubble sizes. However, in order for the continuous and discrete phases to interact, it is necessary to relate the two descriptions. This interaction takes place through three mechanisms:

1. Phase coupling, because each phase occupies a volume not available to the other phase (void fraction coupling)
2. Interface drag between the phases (momentum coupling)
3. Interface energy and mass transfer (energy and mass coupling)

Phase coupling was the most difficult to implement.

Section 2 describes the discrete phase Lagrangian model equations, Section 3 describes the continuous phase Eulerian model equations, Section 4 describes the phase coupling models, Section 5 describes some additional

---

[*] Work supported by the U. S. Department of Energy, Assistant Secretary for Conservation and Renewable Energy, under DOE Field Office, Idaho, Contract DE-AC07-76ID01570. Submitted to the Japan - US Seminar on Two-Phase Flow Dynamics, July 5-11, 1992, Berkeley, CA.

models, Section 6 contains a summary of the basic equations, Section 7 describes test problem calculations that have been performed, and Section 8 contains some conclusions. The references are in Section 9.

In this paper, we only discuss the case of a single discrete phase and a single continuous phase, but work is progressing on the case of two discrete phases and two continuous phases. The results of this work will be reported in due course.

2. DISCRETE PHASE LAGRANGIAN MODEL EQUATIONS

The mass, momentum, energy, and position equations for each bubble are based on the average properties of that bubble. Because each bubble is individually tracked, the bubble conservation equations are ordinary differential equations governing the time evolution of mass, momentum, energy, and position of each bubble. Each of the first three equations includes appropriate interaction terms with the liquid continuous phase through which the bubble is moving.

In the numerical implementation, time derivatives of products are expanded into products of derivatives, and first-order forward differences are used with the coefficients evaluated at the old time level. The conservation equations are written in a partially discretized form that shows the time levels of all the source terms. Terms that contain an n+1 superscript are evaluated at the new time level, and any undifferentiated terms without a time level explicitly shown are evaluated at the old or n^{th} time level. In addition, $\frac{dB}{dt}$ is understood to mean $\frac{B^{n+1} - B^n}{\Delta t}$, where B stands for any variable or combination of variables.

2.1. Bubble Mass Equation

The mass conservation equation for bubble b is,

$$\frac{d(\rho_b V_b)}{dt} = -\Gamma_{bl}^{n+1} \tag{1}$$

where Γ_{bl} is the mass transfer rate from the bubble to the liquid. Because the description of each bubble is Lagrangian, the bubble density, ρ_b, and volume, V_b, are functions of time only.

2.2. Bubble Momentum Equation

The momentum balance for bubble b is,

$$\rho_b V_b \frac{du_b}{dt} = \rho_b V_b g - F_{bl} \tag{2}$$

where the two terms on the right-hand-side are the gravitational body force and the force that the bubble exerts on the continuous phase, F_{bl}. This latter force is the sum of (a) the interphase drag force, (b) the added mass force, and (c) the interface force due to the mean pressure gradient around the bubble,

$$F_{bl} = f_{bl}\left[u_b^{n+1} - \{\bar{u}_l\}_b\right] + C_{al}\{\bar{\rho}_l\}_b V_b\left(\frac{du_b}{dt} - \{\bar{a}_l\}_b\right) + V_b\left[\frac{\partial P}{\partial x}\right]_b \tag{3}$$

where

$$f_{bl} = \left[0.5\{\bar{\rho}_l\}_b C_{db} A_{fb}\left|u_b - \{\bar{u}_l\}_b\right|\right] \tag{4}$$

is the interface drag coefficient, and the overbar signifies an average quantity. The bubble velocity is evaluated implicitly in the interface drag term, which removes the need for small time steps when the interface drag coefficient, f_{bl}, is large.

DISCLAIMER

2.3. Bubble Energy Equation

The energy conservation equation for bubble b is,

$$\frac{d(\rho_b \varepsilon_b V_b)}{dt} = -\varepsilon_b \Gamma_{bl}^{n+1} + \frac{h_b A_{bl}\left(\theta_{bl}^{n+1} - T_b^{n+1}\right)}{\theta_{bl}} \tag{5}$$

which is written in terms of the bubble's entropy, ε_b. The two terms on the right-hand-side are the energy gain from the liquid phase as a result of mass transfer and heat transfer. The bubble-liquid interface temperature, θ_{bl}, is set to the saturation temperature at the location of the bubble.

2.4. Bubble Position Equation

The position equation for bubble b is,

$$\frac{dx_b}{dt} = u_b^{n+1} \tag{6}$$

Equations (1) – (6) are solved for each bubble. Simulations with up to 10,000 bubbles have been made with DISCON on a SGI workstation.

3. CONTINUOUS PHASE EULERIAN MODEL EQUATIONS

The continuous phase equations are discretized using a staggered Eulerian mesh as shown in Figure 1. Mass and energy are conserved in each continuity cell, and momentum is conserved in each momentum cell. The ends of continuity cells are called junctions and are at the centers of the momentum cells. The ends of the momentum cells are at the centers of the continuity cells. Discrete values of density, pressure, and energy are located at the center of the continuity cells, and discrete values of velocity are located at the centers of the momentum cells. In what follows, continuity cells use the index k and momentum cells use the index j. As noted earlier, bubbles use the index b. In the finite difference equations, some variables are needed at locations where they are not defined. Averaging and/or donoring techniques are used to compute these values.

3.1. Liquid Phase Mass Equation

The liquid phase mass conservation equation for volume, V_k, is,

$$\frac{d(\alpha_{kl}\rho_{kl}V_k)}{dt} + \left(A_k \alpha_{kl}\rho_{kl}u_{kl}^{n+1}\right)_{in}^{out} = \sum_{b}^{\substack{bubbles\\ in\,cell\,k}} \left\{\eta_{kb}\Gamma_{bl}^{n+1}\right\} \tag{7}$$

where the average liquid phase velocity at junction j is u_j. The variable η_{kb}, is the fraction of bubble b that is in cell k and is defined in the Volume Fraction Coupling section in terms of the bubble volume, V_b, and location, x_b. In Equation (7), the second term on the left-hand-side represents the net flux of mass out of cell k. As in the bubble equations, the time derivatives are expanded, and first-order forward time differences are used with the coefficients evaluated at the old time level.

To avoid a convective instability due to centered mass flux terms, the fluxed liquid densities in Equation (7) are donored if the velocity is not zero. Because the bubbles are tracked in a Lagrangian manner, there are no instabilities associated with the liquid volume fraction, α_{kl}, and they are not donored.

3.2. Liquid Phase Momentum Equation

The liquid phase momentum conservation equation is,

$$\alpha_{jl}\rho_{jl}V_j \frac{du_{jl}}{dt} + \alpha_{jl}\rho_{jl}V_j u_{jl}\left[\frac{u_{jl} - u_{j-1,l}}{\Delta x}\right] = -\alpha_{jl}V_j\left[\frac{P_k^{n+1} - P_{k-1}^{n+1}}{\Delta x}\right] - f_{jwl}u_{jl}^{n+1} - F_{jbl} + \alpha_{jl}\rho_{jl}V_j g \tag{8}$$

where the four terms on the right-hand-side are the pressure gradient force, the wall friction force, the bubble-liquid interphase drag force, and the gravitational body force.

The bubble-liquid interphase force, F_{jbl}, is defined as,

$$F_{jbl} = -\sum_{b}^{\substack{bubbles\\ in\,cell\,j}} \eta_{jb} F_{bl} \tag{9}$$

where F_{bl} is defined in Equation (3). Consistency between the bubble and the liquid phase momentum interphase force terms must be maintained.

The continuity cell variables with a j subscript are simple averages of neighboring continuity cell values. The convective acceleration terms are evaluated using a one-sided upwind spatial gradient (i.e., donoring to make the convective terms stable). The pressure gradient in the momentum equation and the velocity in the mass equation are both evaluated at new time which makes this scheme implicit in the terms responsible for sound wave propagation. In contrast, explicit schemes have a time step limitation based on sound speed.

3.3. Liquid Phase Energy Equation

The energy conservation equation for the liquid phase in cell k is,

$$\frac{\partial(\alpha_{kl}\rho_{kl}\varepsilon_{kl}V_k)}{\partial t} + \left(A_k\alpha_{kl}\rho_{kl}\varepsilon_{kl}u_{kl}^{n+1}\right)_{in}^{out} = \frac{Q_{wkl}^{n+1}A_{wk}}{T_{wk}} + \sum_{b}^{\substack{bubbles\\ in\,cell\,k}}\left\{\eta_{kb}\Gamma_{bl}^{n+1}\varepsilon_{kl}\right\}$$
$$+ \sum_{b}^{\substack{bubbles\\ in\,cell\,k}}\left\{\eta_{kb}\frac{h_{lb}A_{bl}\left(\theta_{bl}^{n+1} - \left[w_{lb}T_{kl}^{n+1} + (1-w_{lb})T_{wk}^{n+1}\right]\right)}{\theta_{bl}}\right\} \tag{10}$$

which is written in terms of the liquid entropy, ε_{kl}. The second term on the left-hand-side is the net liquid entropy flux out of cell k through its two junctions.

The first term on the right-hand-side is the direct entropy addition rate to the continuous liquid phase from wall heat transfer.

The second term on the right-hand-side is the entropy transfer rate associated with mass transfer from all the bubble-liquid interfaces in cell k to the continuous liquid phase.

The third term on the right-hand-side is the heat transfer rate from all the bubble-liquid interfaces in cell k to the continuous liquid phase. The heat transfer coefficient on the outside of the bubble is h_{lb}. The liquid temperature in cell k varies from the wall temperature to an average bulk temperature. The bubble-liquid heat transfer can occur between the average bulk liquid, which is at the average liquid temperature, T_{kl}, or the wall liquid, which is at the wall temperature, T_{wk}. The weighting factor, w_{lb}, allows us to use a linear combination of these two temperatures to account for bubbles that start on the wall and are later released into the bulk liquid. When w_{lb} is zero, the bubble is surrounded by wall temperature liquid, and when w_{lb} is one, the bubble is surrounded by average temperature liquid. The subcooled boiling model makes use of this feature.

4. PHASE COUPLING MODELS

The coupling of the discrete Lagrangian and continuous Eulerian phases proved to be the most difficult part of the modeling and numerical algorithm development. This section describes the coupling models under three headings: (4.1) volume fraction coupling, (4.2) momentum transfer coupling, and (4.3) energy transfer coupling.

4.1. Volume Fraction Coupling

In two-phase bubbly flow, the bubbles can become quite large due to coalescence, merging to form extended cylindrical bubbles that have transverse diameters approaching the pipe diameter. For this reason, the volume occupied by the bubbles can not be neglected as it frequently is in modeling liquid sprays [4].

The volume of a bubble located at x_b is clearly discrete in space. The volume fraction, α_{kl}, in the continuous liquid phase equations results from these spatially discrete bubble volumes. However, in the continuous phase

equations, the volume fraction is a continuous field variable with a spatially smooth distribution, as in classical two-fluid models like RELAP5 [6] and TRAC [7, 8].

This dual character of the volume fraction means that some smoothing interpolation must be used when the bubble volumes are combined to calculate the continuous phase volume fraction. This has been done in DISCON using an extended bubble shape function. This should not be confused with the actual shape of the bubble, which is described in Section 5.1. The continuous phase model represents the average phase properties over a region of space comparable to the cell length, Δx. Therefore, in order to smooth out this discrete bubble induced continuous phase volume variation, the bubble volume is distributed over an arbitrary length. In the present code, this length is set to the Eulerian cell length, Δx. The code has also run successfully with this arbitrary length set to two or three bubble diameters. Because the bubble locations are Lagrangian, this smoothing does not introduce any artificial diffusion of the volume fraction. It is simply an interpolation of the volume occupied by the discrete bubbles onto the continuous field volume fraction, which is itself an average value over a cell.

The cross-sectional area occupied by an extended bubble at position x and time t is given by, $A_b(x,t)$. It will be convenient when we extend the bubble's length to partition the cross-sectional area into the product of two terms, the bubble's volume, $V_b(t)$, and the bubble's shape, $\eta_b(x,t)$. Since, the integral of the cross-sectional area occupied by a bubble, $A_b(x,t)$, over its length is equal to the bubble's volume, $V_b(t)$, the integral of the bubble's shape over the same length is unity. We also require that the shape function not change as the bubble moves, i.e., the (x,t) dependence of the shape function is only a function, q_b, of the relative distance from the bubble's current position, x_b,

$$\eta_b(x,t) = \eta_b(q_b) = \eta_b[x - x_b(t)] \tag{11}$$

Thus, the bubble's cross-sectional area is,

$$A_b(x,t) = V_b(t)\eta_b[x - x_b(t)] \tag{12}$$

Integrating η_b with respect to x over cell k, we get the fraction of bubble b located in cell k,

$$\eta_{kb}(t) = \int_{cell\,k} \{\eta[x - x_b(t)]\} dx \tag{13}$$

If all of bubble b is in cell k, η_{lb} is equal to unity.

The bubble's volume fraction, α_{kb}, in cell k is the integral of its cross-sectional area over cell k times its volume divided by the volume of cell k,

$$\alpha_{kb}(t) = \left[\frac{V_b(t)}{V_k}\right] \int_{cell\,k} \{\eta[x - x_b(t)]\} dx = \left[\frac{V_b(t)\eta_{kb}(t)}{V_k}\right] \tag{14}$$

The time derivative of the volume fraction with respect to time appears in the liquid phase continuity and energy equations, therefore, we need the time derivative of Equation (14),

$$\frac{d\alpha_{kb}(t)}{dt} = \left[\frac{\eta_{kb}(t)}{V_k}\right]\left[\frac{dV_b(t)}{dt}\right] - u_b(t)\left[\frac{V_b(t)}{V_k}\right] \int_{cell\,k} \left\{\frac{d\eta(q_b)}{dq}\right\} dx \tag{15}$$

where the derivative of $x_b(t)$ with respect to t is the bubble velocity, $u_b(t)$, and the derivative of $q \equiv x - x_b$ with respect to x is 1.

The integral in Equation (15) is written as the difference of the "out" minus the "in" values of η at the two junctions at either end of cell k. From Figure 1, cell k is bounded by junction j on the left and $j+1$ on the right.

$$\frac{d\alpha_{kb}(t)}{dt} = \left[\frac{\eta_{kb}(t)}{V_k}\right]\left[\frac{dV_b(t)}{dt}\right] - u_b(t)\left[\frac{V_b(t)}{V_k}\right]\left[\eta\{x_{j+1} - x_b(t)\} - \eta\{x_j - x_b(t)\}\right] \tag{16}$$

A parallel development for a junction cell leads to a similar expression for α_{jb}.

$$\alpha_{jb}(t) = \left[\frac{V_b(t)}{V_k}\right]\int_{junction\ j}\left[\eta\{x - x_b(t)\}\right]dx = \left[\frac{V_b(t)\,\eta_{jb}(t)}{V_k}\right] \tag{17}$$

Any function can be used for the bubble's shape, $\eta_b(x,t)$, including its actual shape. We use a smooth quartic function in DISCON that has zero first derivatives at both of its end points. This function reduces the perturbations in the liquid phase volume fraction as bubbles move between Eulerian control volumes.

4.2. Momentum Transfer Coupling

The momentum coupling between the bubbles and the liquid is due to the interface force acting on the surface of the bubbles. This force is modeled in the bubble momentum equation by the three terms: (a) interphase drag force, $f_{bl}\left[u_b - \{\bar{u}_l\}_b\right]$, (b) average pressure force, $V_b\,\partial P/\partial x$, and (c) the added mass term. The momentum transfer due to mass transfer was neglected in Equation (8).

The interphase drag force is the classical drag force as measured on a bubble immersed in a liquid. This force is formulated in terms of a drag coefficient, C_d, based on the equivalent frontal area. The drag coefficient is obtained from the data correlations of Peebles and Garber [9] and Harmathy [10]. Peebles and Garber determined the drag coefficient in the laminar and distorted bubble regime and use a four region formula. Harmathy gives an improved formula for the fourth region and adds a fifth formula for the fully turbulent Taylor cap region. These drag coefficient formulas were summarized in a previous paper [11].

When using this formulation for a simulation with many bubbles of various sizes, the question arises of what should be used for the liquid phase far field velocity. In the case of a single bubble rising in a uniform fluid, the appropriate liquid phase far field velocity is clear and is easily determined. In the intermediate situations, the appropriate far field reference velocity is not as well defined. For cylindrical bubbles that nearly fill the pipe, the appropriate far field reference velocity is the liquid phase velocity far ahead of or far behind the bubble. Neglecting compressibility effects, this is equivalent to using the mean volumetric flux as the far field reference velocity. At the other extreme of a single small bubble rising in a large tank, the far field velocity is clearly the liquid velocity far from the bubble, which in the limit of vanishing small bubble size is equivalent to the mean volumetric flux.

In the intermediate cases, where there are many bubbles of various sizes present in the flow, it is necessary to estimate an equivalent far field velocity for use in the drag correlations. Several papers have recently addressed this problem, see Kowe [12] and Couet [13]. A reasonable model for the interstitial far field velocity that takes into account the added mass of the liquid phase displaced with the bubbles has been developed in these references. This model is applicable to low gas volume fraction dispersed flows. When the bubble number density becomes small, the analysis becomes inappropriate. In DISCON, we consider a full range of bubble number densities and bubble sizes including large cylindrical bubbles filling the pipe. We have chosen to use the mean volumetric flux as the far field reference velocity in all situations.

From Equation (17), the volumetric flux at junction j, is,

$$\bar{u}_j = \alpha_j u_j + \sum_{b}^{\substack{bubbles\\ in\,cell\,j}} \alpha_{jb} u_b = \alpha_j u_j + \sum_{b}^{\substack{bubbles\\ in\,cell\,j}} \eta_{jb}\frac{V_b}{V_j} u_b \tag{18}$$

The volumetric far field velocity defined in Equation (18) is independent of position when the liquid and bubble phases are incompressible and there is no mass transfer. In the numerical simulations, it is important to represent this far field velocity with a spatially smooth function independent of the Lagrangian nature of the bubbles. The velocity in Equation (18) is consistent with the far field velocities used when the correlations were developed and gives the spatially smooth reference velocity needed in the drag force calculation.

The far field velocity defined above is not the entire story. Each bubble can also be influenced by the wake of preceding bubbles. A trailing bubble can be "trapped" in the wake of a leading bubble. When a trailing bubble is rising in a liquid and is in the wake of a leading bubble, the trailing bubble is rising in a flow field that has a velocity more nearly equal to that of the leading bubble. In addition, it is rising due to buoyancy in this modified flow field. This is the primary mechanism by which trailing bubbles catch up and coalesce with leading bubbles. This effect is modeled by modifying the far field liquid velocity in Equation (18) by the wake velocity of an appropriate leading bubble when making the drag calculation.

The velocity in the wake of a solid object has been discussed in several texts, see for example Batchelor [14] and Schlichting [15]. In general, for turbulent flow, the wake-induced flow at any position x behind an object can be expressed as,

$$u_{wake} = u_w(x)\exp\left(-\left[\frac{r}{r_w(x)}\right]^2\right) \tag{19}$$

where $u_W(x)$ is the centerline wake velocity, and $r_W(x)$ is a scale for the radial distribution of the wake velocity. A standard integral momentum balance gives the following relationship between $u_W(x)$ and $r_W(x)$,

$$\left[\frac{u_w}{u_r}\right]\left[\frac{r_w}{r_p}\right]^2 = \frac{1}{2}C_d \tag{20}$$

where u_r is the velocity of the wake producing object relative to the fluid, and r_b is the equivalent radius of the object based upon a spherical shape consistent with the calculation of C_d.

Using Equations (19) and (20), the velocity at any location behind an object caused by its wake can be found if we know $u_W(x)$ or $r_W(x)$. Stuhmiller [5] has carried out a preliminary correlation of wake centerline velocity data from several sources and gives the following formula for $u_W(x)$,

$$\left[\frac{u_w}{u_r}\right] = \left[a_w + b_w\left(\frac{x}{R_b}\right) + \left(\frac{x}{R_b}\right)^2\right]^{-1} \tag{21}$$

where $a_W = 0.20$, $b_W = 0.12$, $c_W = 0.01$, and R_b is the actual radius of the object.

To complete the wake model, the wake velocity of every bubble leading a trailing bubble is calculated. Two wake models are used in the DISCON code. The "maximum" wake model uses the maximum of all the leading bubble wakes for the trailing bubble, and the "closest" wake model uses the wake of the closest leading bubble for the trailing bubble. In both cases, the leading bubble's wake velocity is used to calculate the modified far field velocity, $\{\overline{u}_l\}_b$, for the trailing bubble.

The second momentum coupling term, $V_b\,\partial P/\partial x$, represents the pressure force on the bubble's surface due to the mean pressure gradient in the liquid phase. This is the source of the buoyancy term for a bubble in a stagnant fluid under the action of gravity. In the present version of DISCON, this effective mean pressure gradient in the liquid phase is modeled using the gravity head and inertial acceleration of the far field continuous liquid phase flow,

$$\frac{\partial \overline{P}}{\partial x} = \{\overline{\rho}_l\}_b\left[g - \left(\frac{\partial\{\overline{u}_l\}_b}{\partial t} + \{\overline{u}_l\}_b\frac{\partial\{\overline{u}_l\}_b}{\partial x}\right)\right] \tag{22}$$

where $\{\overline{\rho}_l\}_b$ is the liquid density at the location of bubble b.

The third momentum coupling term, added mass, is modeled in the conventional manner using an added mass coefficient of 0.5.

4.3. Energy Transfer Coupling

The energy transfer between the bubble and liquid is due to heat transfer and mass transfer. Since there can be no accumulation of energy in the bubble-liquid interface, the sum of the energy entering and leaving the interface must equal zero.

$$-\varepsilon_b\Gamma_{bl}^{n+1} + \frac{h_b A_{bl}\left(\theta_{bi}^{n+1} - T_b^{n+1}\right)}{\theta_{bl}} + \varepsilon_{lb}\Gamma_{bl}^{n+1} + \frac{h_{lb}A_{bl}\left(\theta_{bl}^{n+1} - \left[w_{lb}T_{lb}^{n+1} + (1-w_{lb})T_{wb}^{n+1}\right]\right)}{\theta_{bl}} = 0 \tag{23}$$

where the first two terms are for the inside of the bubble, and the last two terms are for the outside of the bubble.

The first term is the entropy addition rate from the inside of the bubble to the bubble-liquid interface as a result of mass transfer. The second term is the entropy addition rate from the inside of the bubble to the bubble-liquid interface as a result of heat transfer. The third term is the entropy addition rate to the interface from the surrounding liquid as a result of mass transfer. The last term is the entropy addition rate from the surrounding liquid to the interface as a result of heat transfer. As in Equation (10), the surrounding liquid can be at any temperature between the wall temperature and the bulk liquid temperature.

In Equation (23), we introduced three new variables, ε_{lb}, T_{lb}, and T_{wb}. These define the average liquid entropy, average liquid temperature, and average wall liquid temperature surrounding bubble b in cell k,

$$\varepsilon_{lb} = \sum_{\substack{k \\ \text{cells containing bubble } b}} \left[\eta_{kb} \varepsilon_{kl} \right] \tag{24}$$

Analogous equations define T_{lb} and T_{wb}.

5. ADDITIONAL MODELS

Bubble coalescence requires a model for computing the bubble shapes. In addition, models are needed for bubble turbulence and bubble-liquid heat transfer. We need film heat transfer coefficients on the inside and outside of the bubble-liquid interface.

5.1. Bubble Shape Model

So far in the development, the actual shape of the bubble has not been a factor in the model. While the drag coefficient depends the shape of the bubble, the shape of the bubble is determined by the volume of the bubble. Therefore, the drag correlations were based upon the frontal area of an equivalent sphere having volume V_b, and the actual shape was not needed. In general, bubbles take on a variety of shapes depending upon their size. The sequence of shapes shown in Figure 2 is generally characterized in increasing volume as a sphere, oblate spheroid, Taylor cap, and cylindrical bubble or slug.

DISCON uses the formulas given by Stuhmiller [5] to characterize these shapes. These formulas are based upon the bubble volume, V_b, the pipe radius, R, and the Eötvös number, Eo, which is defined as,

$$\mathrm{Eo} = 4 g r_{eq}^2 \left[\frac{|\rho_b - \rho_{kl}|}{\sigma} \right] \tag{25}$$

where r_{eq} is the equivalent spherical radius of a bubble having volume V_b.

These shapes are explicitly used at two places in the model and in all visual output from a DISCON simulation. The body or actual radius of the bubble, R_b, is used in the wake centerline velocity calculation, Equation (21). Both the bubble body radius, R_b, and the actual vertical height of a bubble are used in the bubble coalescence model.

5.2. Bubble Coalescence Model

If two bubbles overlap in the radial and axial directions by more than a prescribed overlap fraction, they are merged or coalesced. The bubble shapes are used in the computation of this overlap fraction, which is an input parameter. In most simulations, the overlap fraction is zero, i.e., the two bubbles merge when they just touch. When two bubbles are merged, the sum of their masses, momenta, and entropies are preserved. The merged bubble is placed at the center of mass of the two original bubbles. Only bubbles in the free stream are merged. All bubbles attached to the wall, i.e., nucleating bubbles from subcooled boiling, retain their identity even if they overlap another bubble. They are only merged after they grow large enough to be released from the wall.

5.3. *Wall Heat Transfer Model*

Wall heat transfer models were developed for forced convection, subcooled boiling, and saturated boiling. The forced convection and saturated boiling models are conventional, but the subcooled boiling model is new and will be explained in more detail.

In subcooled boiling, the average liquid temperature is less than the saturation temperature, so in theory, no boiling can take place. However, if the wall heat flux is large enough, the wall temperature will be above the saturation temperature, the liquid adjacent to the wall will be above the saturation temperature, and subcooled boiling can take place. The subcooled boiling model partitions the heat flux into two parts: (a) that driven by the difference in the wall temperature and the bulk liquid temperature, and (b) that driven by the difference in the wall temperature and the liquid saturation temperature. In the subcooled boiling model, a portion of the heat goes into heating up the liquid phase, and the remainder goes into creating and growing bubbles that are attached to the wall. Once the bubbles reach a critical size, they are released into the bulk liquid phase where they can either grow or condense.

For the wall heat flux to the liquid, we have,

$$Q_{wkl}^{n+1} = h_{kl,mic}\left[T_{wk}^{n+1} - \tilde{T}_{sat}\left(P_k^{n+1}\right)\right] + h_{kl,mac}\left[T_{wk}^{n+1} - T_{kl}^{n+1}\right] \tag{26}$$

where the heat transfer coefficients are taken from the Chen correlation [16]. In DISCON, the wall heat flux is an input quantity, so Equation (26) is used to determine the wall temperature.

5.4. *Inside the Bubble-Liquid Heat Transfer Model*

The bubble–liquid heat transfer model consists of two models: (a) one for the inside of the bubble and (b) one for the outside of the bubble. The outside heat transfer model is further modified when the bubble is attached to the wall at a boiling nucleation site.

Inside the bubble, we use a relaxation model to compute the heat transfer coefficient,

$$H_b \equiv \left[\frac{h_b A_{bl}}{\theta_{lb}}\right] = \left[\frac{V_b \rho_b}{\tau_{hb}}\right]\left[\frac{\partial \varepsilon_b}{\partial T}\right]_P \tag{27}$$

where τ_{hb} is the relaxation time constant for the bubble temperature. The relaxation time constant is the time it takes the bubble temperature to come within about 63% of its final value after a step change in the bubble-liquid interface temperature. After about five relaxation time constants, the bubble temperature is within 99% of the bubble-liquid interface temperature. This relaxation time constant is input and in most calculations is set to 20% of the time step to assure that the bubble temperature stays close to the saturation temperature at each time step.

5.5. *Outside the Bubble-Liquid Heat Transfer Model*

Outside the bubble, when it is in the free stream, i.e., not attached to a wall nucleation site, we use a heat transfer model from Whitaker [17] for heat transfer to a sphere in a flowing fluid,

$$H_{lb} \equiv \left[\frac{h_{lb} A_{bl}}{\theta_{bl}}\right] = \left[\frac{A_{bl}}{\theta_{bl}}\right]\left[\frac{k_l}{2R_{eq_b}}\right]\left[2 + \left(0.4\,\mathrm{Re}_b^{0.5} + 0.06\,\mathrm{Re}_b^{0.67}\right)\mathrm{Pr}_b^{0.4}\right] \tag{28}$$

where Re_b, is the bubble's Reynolds number that is based on bubble's relative velocity and Pr_b, is the bubble's Prandl number.

When the bubble is attached to a wall nucleation site, we compute an equivalent heat transfer coefficient from a combination of Lahey's model [18] for subcooled boiling, Saha and Zuber's correlation [19] for the critical enthalpy for net generation of vapor, and the Chen correlation [16].

The partitioning of the heat transferred from the wall into the growing of bubbles and heating of liquid is taken from Lahey's model [18] for subcooled boiling. The mass transfer rate from the liquid adjacent to the wall to a bubble on the wall is given by,

$$\Gamma_{wkb} = \frac{Q_{wkl} A_{wk} M_{kl}}{\left[\hat{i}_{g,sat}(P_k) - i_{kl}\right]} \tag{29}$$

where M_{kl} is a multiplier that gives the fraction of the wall heat flux that goes to making bubbles. The multiplier involves thermodynamic quantities and a net generation critical enthalpy that is given by the Saha-Zuber model [19].

We can now modify the Chen correlation for the film heat transfer coefficient on the liquid side for bubbles on the wall, $h_{kl,mic}$, so that we get the mass transfer rate given in Equation (29). This way, the code will automatically compute the correct amount of mass to transfer from the liquid phase to the bubbles attached to the wall. For this special case, the conservation of energy at the bubble-liquid interface, Equation (23), can be simplified to,

$$(\varepsilon_b - \varepsilon_{lb})\Gamma_{bl} = H_{lb}(\theta_{bl} - T_{wb}) \tag{30}$$

where we set w_{lb} to zero because the bubble is on the wall, and I_b to θ_{bl} because the bubble is small so its internal temperature cannot differ very much from its interface temperature, θ_{bl}. We also combined three variables, $h_{lb}A_{bl}/\theta_{bl}$, into one variable, H_{lb}.

Substituting Equation (29) for Γ_{wkb} into Equation (30) for Γ_{bl}, we get,

$$\frac{Q_{wkl} A_{wk} M_{kl}(\varepsilon_b - \varepsilon_{lb})}{N_{kl}\left[\hat{i}_{l,sat}(P_k) - i_{kl}\right]} = H_{lb}(\theta_{bl} - T_{wb}) \tag{31}$$

where N_{kl} is the number of bubbles attached to the wall in cell k. By dividing by N_{kl}, we assumed that the bubbles attached to the wall have equal rights and get an equal share of the wall heat flux.

Substituting for the wall heat flux to the liquid, Q_{wkl} from Equation (26), and noting that the saturation temperature in this equation, T_{sat}, is the same as the interface temperature, θ_{bl}, and for small bubbles, the temperature of the liquid surrounding a bubble, T_{wb}, is close to the wall temperature, T_{wk}, we can write Equation (31) as,

$$\left\{\frac{A_{wk} M_{kl}(\varepsilon_b - \varepsilon_{lb})}{N_{kl}\left[\hat{i}_{l,sat}(P_k) - i_{kl}\right]}\right\}\left\{h_{kl,mic}\left[T_{wk} - \theta_{bl}\right] + h_{kl,mac}\left[T_{wk} - T_{kl}\right]\right\} = H_{lb}(\theta_{bl} - T_{wk}) \tag{32}$$

Solving this equation for H_{lb}, we get,

$$H_{lb} \equiv \frac{h_{lb}A_{bl}}{\theta_{bl}} = -\left\{\frac{A_{wk} M_{kl}(\varepsilon_b - \varepsilon_{lb})}{N_{kl}\left[\hat{i}_{l,sat}(P_k) - i_{kl}\right]}\right\}\left\{h_{kl,mic} + h_{kl,mac}\left[\frac{T_{wk} - T_{kl}}{T_{wk} - \theta_{bl}}\right]\right\} \tag{33}$$

When this value for H_{lb}, is used for a bubble attached to a wall nucleation site, sufficient energy and mass will be transferred from the liquid to the bubble such that the same void fraction will be created as would have been produced by the original set of correlations.

While this subcooled boiling model for H_{lb} is somewhat unconventional, it is used here because we have not found any appropriate correlations for the heat transfer coefficient on the outside of bubbles attached to wall nucleation sites. However, the DISCON code is certainly capable of using such correlations if and when they become available.

6. SUMMARY OF BASIC EQUATIONS

For the bubbles, the basic conservation equations are for mass, (1), momentum, (2), and energy, (5), along with the bubble position equation, (6). For the liquid, the basic conservation equations are for mass, (7), momentum, (8), and energy, (10). In addition, there is the energy transfer coupling equation, (23). These eight equations (per bubble, per cell) are the basic equations to be solved for the eight new time variables, V_b, u_b, ε_b, x_b, P_k, u_{jl}, ε_{kl}, and Γ_{bl}. The formulas of Section 4.1 are used to express the volume fraction, α_{kl}, in terms of the bubble volume, V_b. The new time value of the bubble density, ρ_b, is a function of the independent state

variables, P_k, T_b, and new time value of the liquid density, ρ_{kl}, is a function of the independent state variables, P_k and T_{kl}. The present version of the code neglects any pressure difference between the phases; therefore, P_k, when interpolated to a bubble position, forms an independent state variable for the bubble phase. All state relationships are linearized over a time step.

An examination of the finite difference equations reveals the following:

- The equations are linear in the new time variables. Hence, each time advancement only requires the solution of a linear system of equations. This is a very complicated linear system due to the mixed Lagrangian and Eulerian features of the equations and the implicit coupling between the bubbles and the liquid phase caused by the time derivatives of α_k in Equations (7) and (10). This linear system of equations is solved using Gaussian elimination.
- The acoustic terms i.e., velocities in Equation (7) and pressure gradient in Equation (8), are evaluated implicitly; hence, there is no stability restriction on the time step size due to acoustic wave propagation.
- The drag term in the bubble momentum equation is evaluated implicitly in u_b. Hence, the short time constant associated with a large drag force on the bubble does not lead to a stability restriction on the time step size.

Because of the explicit evaluation of the convective terms in the continuous liquid phase, there is a stability restriction on the time step size, which is the material Courant limit. In addition to this, the time step size must be chosen small enough to accurately resolve the important physics of the process.

7. TEST PROBLEMS

This section contains comparisons of DISCON calculations of three experiments: (a) Crabtree and Bridgwater bubble coalescence experiment, (b) JAYCOR bubbly air-water flow experiment, and (c) Carl St. Pierre subcooled boiling experiment.

7.1. Crabtree and Bridgwater Experiment

Crabtree and Bridgwater [20] conducted experiments in which they bubbled air into the bottom of a large tank containing a viscous liquid and studied the coalescence of a trailing bubble with a leading bubble. They measured the relative motion of vertically aligned bubble pairs, each having volumes from 10 cm^3 to 40 cm^3, in a 67 % by weight solution of sucrose in water. The Reynolds numbers based on bubble diameters were in the range of 40-90. The Crabtree and Bridgwater experimental data were used to check the drag coefficient model for single bubbles and for evaluating the wake velocity model for two successive bubbles.

DISCON was used to calculate one Crabtree and Bridgwater experiment in which a leading 30 cm^3 bubble was trailed by a 25 cm^3 bubble. The rise of the leading bubble is essentially unaffected by the trailing bubble, and hence, has a constant velocity as seen in Figure 3. Figure 3 also shows a plot of distance vs. time for the trailing bubble from the experiment.

Using Equation (21) with a_W = 0.20 as recommended by Stuhmiller [5], we see from Figure 3 that the DISCON calculation of the trailing bubble's path deviates from the experimental data as it approaches the leading bubble. With a_W = 0.20, we predict that the trailing bubble merges with the leading bubble at 0.65 s. However, in the experiment, the time at which the two bubbles merged was closer to 0.8 s. We then modified the centerline wake induced velocity correlation given in Equation (21) for small separation distances by increasing a_W from 0.20 to 0.45. With this change, we obtained much better agreement with the experimental data.

There was a wide scatter in the data points that were used by Stuhmiller in obtaining his original centerline wake velocity correlation. When the modified correlation was plotted over the data, it appears to fit the data about as well did the original correlation. All further calculations were made with a_W = 0.45.

7.2. *JAYCOR Bubbly Air-Water Experiment*

The model embodied in DISCON is inherently statistical. Because individual bubbles are tracked, two different simulations with different bubble volume and velocity distributions can have similar average values for the volume fraction, mean bubble velocity, etc. Every simulation with DISCON is in effect a new experiment when the bubble distribution is re-initialized, even if the mean values of the new initialization are identical with the original. Many experiments have been performed on bubbly air-water flows, but almost all report only selected mean values.

Stuhmiller from JAYCOR in connection with the development of their BUBBLE code performed an air-water experiment in which fairly detailed statistical data were gathered. In this experiment, air was bubbled up a vertical water-filled pipe, and movies were taken at various axial elevations. At each elevation, the volume and velocity of each passing bubble was measured and recorded. These volumes and velocities were then grouped into a set of bins. For example, all bubbles having velocities between 20 cm/s and 22 cm/s were included in the 21 cm/s velocity bin, and all bubbles having volumes between 10 cm^3 and 12 cm^3 were included in the 11 cm^3 volume bin. Since the raw data was not available, the data from the plots that were published in the EPRI report [10] was digitized and used for our comparisons with the DISCON calculations. The JAYCOR experiment consisted of a 1.27 cm radius circular pipe having a length of 140 cm. The top of the pipe was open, and air was bubbled into the bottom at a flow rate of 22.4 cm^3/s.

The pipe was modeled with DISCON using 17 volumes. A time step of 10 ms was used. With this size time step, a bubble moving at 50 cm/s, which is an upper limit, would take about 16 time steps to move through a cell. Because of the statistical nature of the DISCON model, we used an initial transient period of 100 s, and then gathered numerical data during the following 100 s.

Figure 4 shows a series of frames, spaced every 5 time steps, of the simulated DISCON calculation in the entire pipe. The first frame is on the left, and frame numbers increase across the page. This figure illustrates the bubble merging that occurred in this experiment.

The bubble volume data for a typical JAYCOR experiment and the corresponding DISCON calculation are shown in Figure 5. This figure shows both the mean bubble volume and standard deviation, sigma, at various elevations.

The experimental data show a systematic evolution of the flow regimes with elevation. As the bubbles move up the pipe, they merge causing the mean of the volume distribution to shift to larger and larger values. This is shown in Figures 4 and 5. As can be seen from Figure 5, the experimental data show an increasing spread in the bubble volume, i.e., standard deviation, with elevation. Close to the orifice, bubbles are all the same size, while at the higher elevations, some bubbles have merged to give larger bubbles while other bubbles remain at their original size, which results in a larger spread in the bubble volumes.

The numerical simulation shows fairly good agreement with a slight underprediction of bubble volume at the lower elevations and a slightly higher bubble volume predicted at the higher elevations. There must be more merging occurring in the middle of the pipe in our simulation than in the experiment. It should be noted that DISCON predicted a growth in the standard deviation that parallels the data trend quite accurately given the statistical nature of the data and simulation.

Figure 6 shows the mean and standard deviation of the bubble velocities for both the data from the experiment and the data from the DISCON calculation. The mean bubble velocities are slightly overpredicted by DISCON, which is consistent with the volume data. The large mean bubble velocities at the lower elevations is due to the wake model. A trailing bubble in the wake of a leading bubble can move 2-3 times faster than the leading bubble.

It should be noted that while the initial bubbles have an oblate spheroidal shape, they quickly merge to form a Taylor cap shape, and then merge again to form cylindrical bubbles or slugs. Slugs in this size pipe move at a constant velocity of about 18 cm/s. This singular velocity of a slug is evident in the asymptotic character of the mean velocity curves at higher elevations. The mean velocity decreases with increasing axial elevation in the pipe. From this figure, we can see that there are still some smaller bubbles or Taylor caps at the higher elevations of the pipe. The spread in the bubble velocity is almost constant with a slight decrease with elevation because of the constant velocity of the slug. The calculated standard deviation in bubble velocity is somewhat larger than that from the experimental data.

7.3. St. Pierre Subcooled Boiling Experiment

For his Ph.D. thesis [21], Carl St. Pierre made measurements of the void distribution at numerous elevations in a rectangular channel that was electrically heated. Water flowed up the channel, and subcooled boiling occurred on the walls. St. Pierre computed the average void fraction from his void distribution data.

DISCON was used to calculate Run 10 of Carl St. Pierre's experiment. Run 10 had the highest inlet subcooling of 7.0 K. It had a pressure of 4.14 MPa, and an inlet velocity of 1.152 m/s. The wall heat flux was 2.88×10^5 W/m^2. The channel was rectangular and had dimensions of 1.11 x 4.445 cm. The heated length was 125.7 cm, and the total length was 154.9 cm. A power supply that could output 100 V at 3000 A supplied the heating. The void fraction measurements used the gamma-ray attenuation technique. St. Pierre estimated the error in the average void fraction at less than 10%. Measurements were made at thirteen equidistant locations along the channel, and in all cases, the gamma-ray beam passed through the 4.445 cm depth of the channel. Traversal of the channel in the narrow direction provided void fraction measurements across the channel at nine locations. These were averaged to get the average void fraction data at each of the thirteen axial locations. Due to small misalignments, only 80% of the cross section could be traversed. St. Pierre states that this limitation would tend to give higher void fractions for the downstream portion of the test section where convex void fraction distributions were present and lower fractions near the inlet where concave distributions were present.

We modeled the experiment with 10 cells in the heated section with 2 cells on either end for a total of 14 cells. Time steps of 5 ms were used. The water was initialized with a uniform pressure and temperature. The wall heat flux was turned on at cycle 5 which was after the gravity head in the water had built up. The calculation was 500 cycles long (2.5 s), and steady state was reached at 300 cycles (1.5 s). Bubbles were released from the wall when their radius exceeded 1 mm. Their initial radius was 0.001 mm. The runs were made with 10 active nucleation sites per cell on the wall. The wall nucleation sites were randomly selected.

Figure 7 shows a comparison of the DISCON calculation with the experimental data. We added ±10% error bars onto the experimental data, as recommended by St. Pierre. The data for the calculation are averaged over the last 100 cycles (0.5 s). The calculated void has a general tendency to be under the experimental data at the higher elevations. This difference could be attributed to the fact that the average of the experimental data was higher than it should be as a result of not averaging in the low void fractions near the wall. St. Pierre was able to only measure the void fraction from the center to 80% of the channel width. The measured void fraction at 80% of channel width is half of the average, so the low void fractions near the wall at the higher elevations would have lowered the average.

Figure 8 shows the total number of bubbles in the channel at each cycle of the calculation. Since we activated 10 nucleation sites in each of the 10 cells, 100 of these bubbles were on the wall at nucleation sites. That leaves about 1100 bubbles in the free stream after the initial peak of 2250 bubbles has subsided (after cycle 100) None of the bubbles released from the wall collapsed in the free stream. Evidently, the subcooling was not large enough, and they coalesced with existing bubbles in the free stream before they had time to collapse. The fluctuation in the number of bubbles gives an indication of the statistical nature of the calculation. A repeat of this calculation with a different set of wall nucleation sites would result in a different number of bubbles at each cycle.

Figure 9 shows the liquid, wall, and saturation temperatures for the DISCON calculation. Since the wall heat flux is constant and the wall temperature is almost parallel to the saturation temperature, we see that the h_{mic} portion of the Chen correlation is the dominating term in the wall temperature model. There is some slight curvature of the wall temperature at the entrance, which indicates that if the subcooling was larger, the h_{mac} portion of the Chen correlation would come into play and the wall temperature would parallel the liquid temperature. (See Figure 5.1 in Collier [22]).

8. CONCLUSIONS

The discrete-bubble two-phase flow model is able to dynamically predict the evolution of both the flow topology and energy partitioning as the bubbles form on the wall and merge due to wake effects. Many more simulations are required, however, including larger subcooling experiments and the transition from long cylindrical bubbles to annular flow. Our goal is to be able to simulate a boiling experiment that has subcooled water at the entrance and superheated steam at the exit. However, before this simulation can be done, we need to add the second continuous gas phase with its discrete drops. We also need to improve the heat transfer models for bubbles attached to wall nucleation sites. Work along these lines is in progress.

9. REFERENCES

[1] J.K. Dukowicz, Quasi-Steady Droplet Phase Change in the Presence of Convection, Technical Report LA-7997-MS, Los Alamos Scientific Laboratory, Los Alamos, NM (August 1979).

[2] P.J. O' Rourke, Collective Drop Effects in Vaporizing Liquid Sprays, Ph.D. Thesis, No. 1532-T, Princeton University, Princeton, NJ (November 1981).

[3] P.J. O' Rourke and A.A. Amsden, The Tab Method for Numerical Calculation of Spray Droplet Breakup, In International Fuels and Lubricants Meeting and Exposition, Toronto, Ontario, Society of Automotive Engineers (November 1987).

[4] A.A. Amsden, P.J. O' Rourke, and T.D. Butler, KIVA-II: A Computer Program for Chemical Reactive Flows with Sprays, Technical Report LA-11560-MS, Los Alamos National Laboratory, Los Alamos, NM (May 1989).

[5] J.H. Stuhmiller, R.E. Ferguson, and C.A. Meister, Numerical Simulation of Bubbly Flow, Technical Report EPRI NP-6557, Electric Power Research Institute, Palo Alto, CA (November 1989).

[6] V.H. Ransom, et. al., RELAP5/MOD2 Code Manual, Technical Report NUREG/CR-4312 and EGG-2396, EG&G Idaho (August 1985).

[7] LANL Nuclear Saftey Code Development Group, TRAC-PD2, An Advanced Best Estimate Computer Program for Pressurized Water Reactor Loss-of-Coolant Accident Analysis, Technical Report LA-8709-MS, NUREG/CR-2054, Los Alamos National Laboratory (April 1981).

[8] D.D. Taylor, et. al., TRAC-BD1/MOD1: An Advanced Best Estimate Computer Program for Boiling Water Reactor Transient Analysis, Technical Report NUREG/CR-3633 and EGG-2294, EG&G Idaho (April 1984).

[9] F.N. Peebles and H.J. Garber, Studies in the Motion of Gas Bubbles in Liquids, Chem. Engr. Progress, Vol. 49 (1953) pp. 88–97.

[10] T.Z. Harmathy, Velocity of Large Drops and Bubbles in Media of Infinite or Restricted Extent, AIChE J., Vol. 6 (1960) pp. 281–288.

[11] J.A. Trapp, G.A. Mortensen, and V.H. Ransom, Particle-Fluid Two-Phase Flow Modeling, In Advances in Mathematics, Computations, and Reactor Physics, American Nuclear Society (April 1991).

[12] R. Kowe, J.C.R. Hunt, A. Hunt, B. Couet, and L.J.S. Bradbury, The Effects of Bubbles on the Volume Fluxes and the Pressure Gradients in Unsteady and Non-Uniform Flow of Liquids, Int. J. Multiphase Flow, Vol. 14 (1988) pp. 587–606.

[13] B. Couet, P. Brown, and A. Hunt, Two-Phase Bubbly-Droplet Flow through a Contraction: Experiments and a Unified Model, Int. J. Multiphase Flow, Vol. 17 (1991) pp. 291–307.

[14] G.K. Batchelor, An Introduction to Fluid Dynamics (Cambridge at the University Press, London, 1967).

[15] H. Schlichting, Boundary Layer Theory (Pergamon Press, New York, 1955) Translated by J. Kestin.

[16] J.C Chen, Correlation for Boiling Heat Transfer to Saturated Fluids in convective Flow, I & E C Process Design and Development, Vol. 5 (July 1966) pp. 322–329.

[17] S. Whitaker, Forced Convection Heat-Transfer Correlations for Flow in Pipes, Past Flat Plates, Single Cylinders, Single Spheres, and Flow in Packed Beds and Tube Bundles, AIChE J., Vol. 18 (1972) pp. 361.

[18] R.T. Lahey, A Mechanistic Subcooled Boiling Model, In Proceedings of the Sixth International Heat Transfer Conference in Toronto, Canada, ASME (1978) pp. 293–295.

[19] P. Saha and N. Zuber, Point of Net Vapor Generation and Vapor Void Fraction in Subcooled Boiling, In Proceedings of the 5th International Heat Transfer Conference, Tokyo, ASME (1974).

[20] J.R. Crabtree and J. Bridgwater, Bubble Coalescence in Viscous Liquids, Chem. Engr. Sci., Vol. 26 (1971) pp. 839–851.

[21] C.C. St Pierre, Frequency Response Analysis of Steam Voids to Sinusoidal Power Modulation in a Thin Walled Boiling Water Coolant Channel, Ph.D. Thesis, Northwestern University (1965).

[22] J.G. Collier, Convective Boiling and Condensation (McGraw-Hill, 1972).

NOMENCLATURE

a = acceleration (m/s^2)

a_w = wake velocity fitting coefficient

A = area (m^2)

b_w = wake velocity fitting coefficient

B = any variable or any combination of variables

c_w = wake velocity fitting coefficient

C = coefficient (added mass or drag)

Eo = Eötvös number

f = interface or wall drag coefficient (kg/s)

F = force bubble exerts on continuous phase (N)

g = acceleration of gravity (m/s^2)

h = film heat transfer coefficient (J/m^2-s-K)

H = hA/θ ($J/s\text{-}K^2$)

i = enthalpy (J/kg)

k = conductivity (J/s-m-K)

M = multiplier

N = number

P = pressure (Pa)

Pr = Prandl number

q = $x - x_b$ (m)

Q = heat flux per unit area(J/m^2-s)

r = radial or radius (m)

R = radius (m)

Re = Reynolds Number

t = time (s)

T = temperature (K)

u = velocity (m/s)

V = volume (m^3)

w = temperature weighting factor

x = distance (m)

Greek Symbols

α = volume fraction

Δ = increment

ε = entropy (J/kg-K)

Γ = mass transfer rate (kg/s)

η = fraction of a bubble

σ = surface tension (N/m)

τ = relaxation time constant (s)

θ = interface temperature (K)

ρ = density (kg/m^3)

Subscripts

a = added mass

b = bubble index or body

d = drag

eq = equivalent

f = frontal

g = gas

j = momentum cell index

k = continuity and energy cell index

l = liquid

mac = macroscopic (Chen correlation)

mic = microscopic (Chen correlation)

p = particle or body

sat = saturation

w = wall or wake

$wake$ = wake

Superscripts

n = n^{th} time level

$\bar{}$ = overbar signifies an average

FIGURES

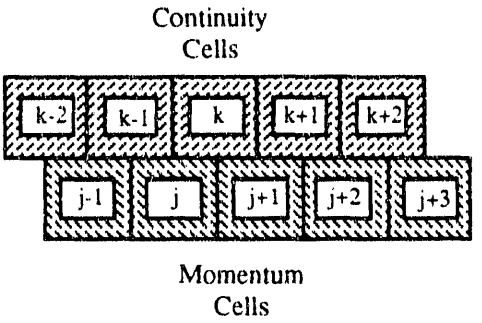

Figure 1. Continuity and Momentum Cell Locations for the Staggered Eulerian Grid.

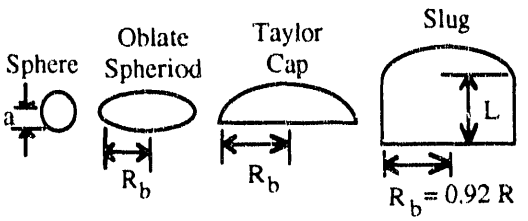

Figure. 2. Calculated Bubble Shapes.

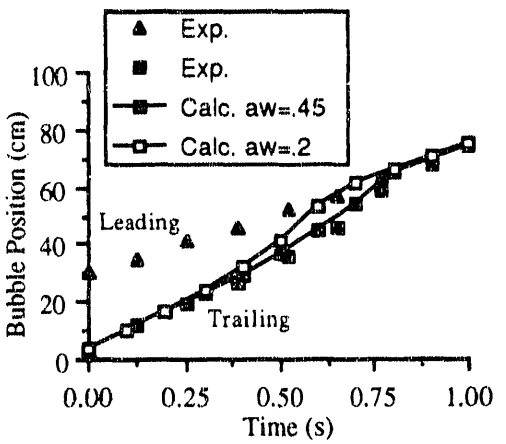

Figure 3. Position vs. Time of Leading and Trailing Bubbles in Crabtree and Bridgwater Comparison.

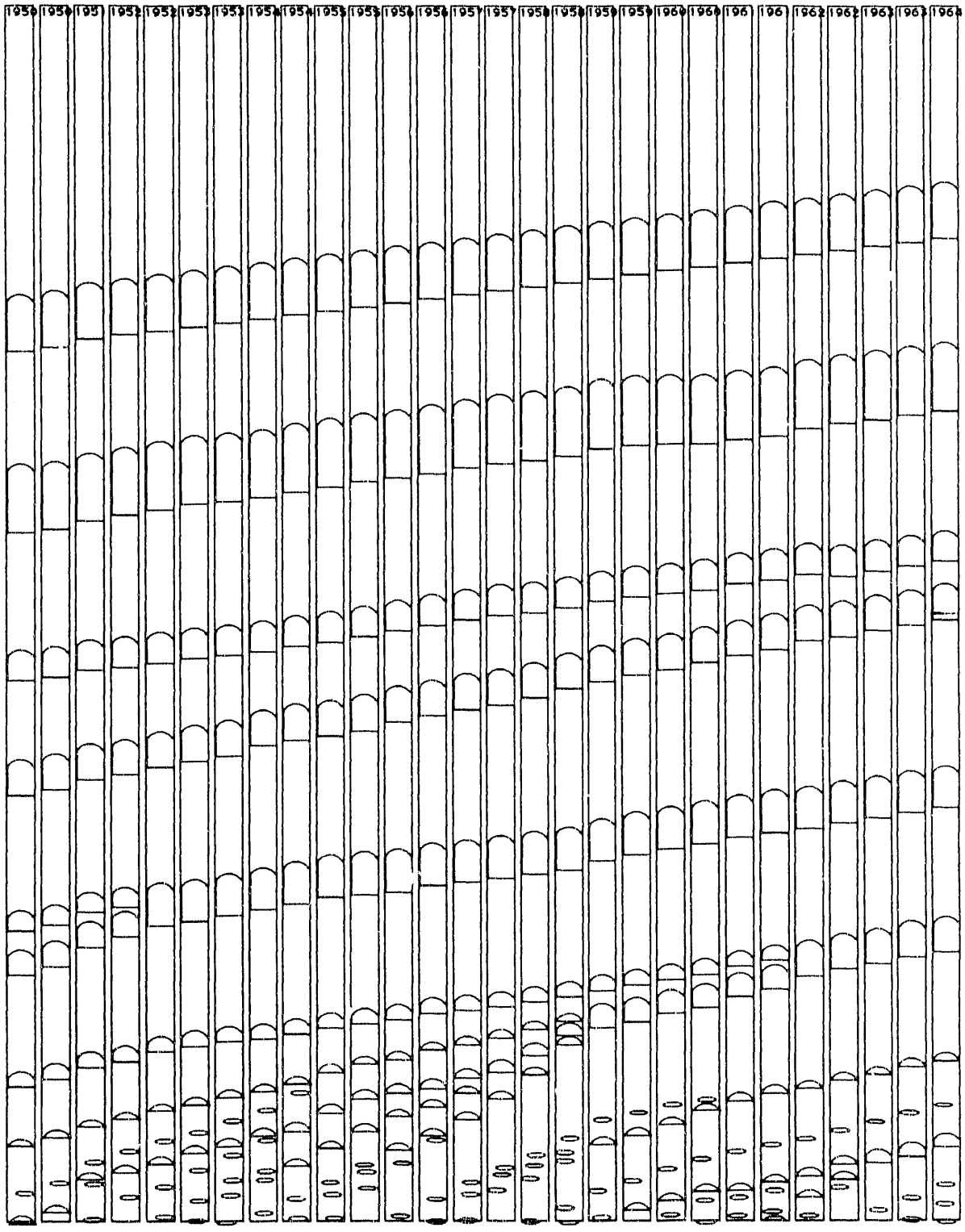

Figure 4. Calculated Bubble Shapes Near the End of the JAYCOR Simulation.

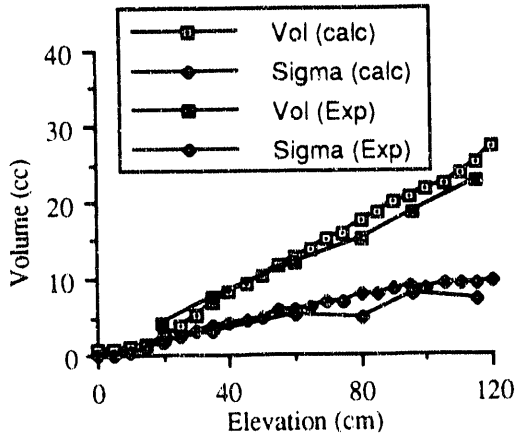

Figure 5. JAYCOR Experiment and DISCON Simulation, Bubble Volume and Sigma vs. Axial Elevation.

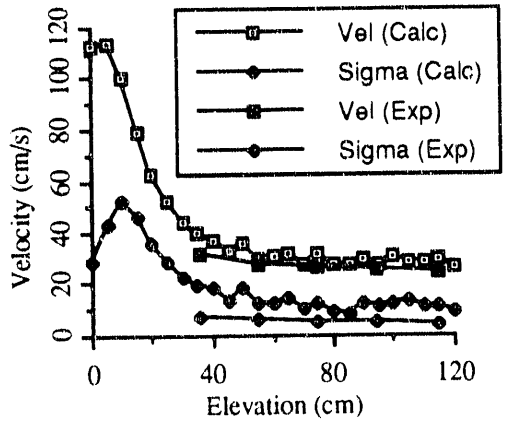

Figure 6. JAYCOR Experiment and DISCON Simulation, Bubble Velocity and Sigma vs. Axial Elevation.

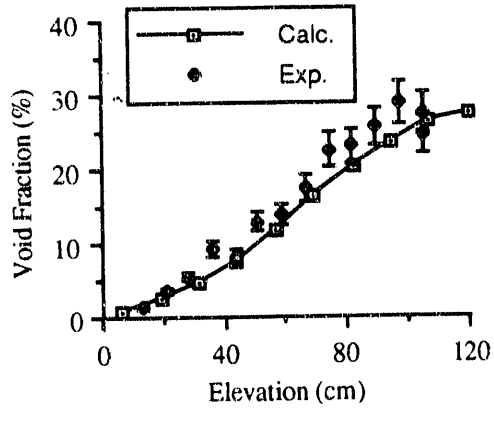

Figure 7. Comparison of Averaged Void Fraction for St. Pierre Run 10 and DISCON Calculation.

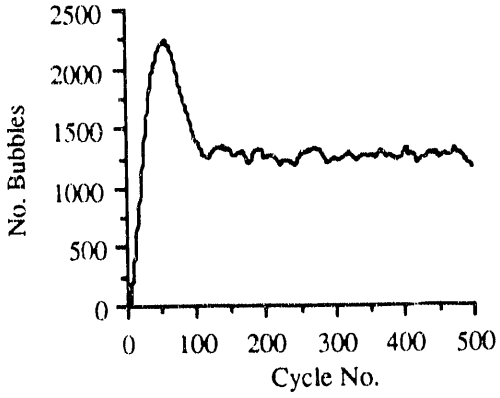

Figure 8. Total Number of Bubbles in the Channel for the DISCON Simulation of the St. Pierre Experiment Run 10.

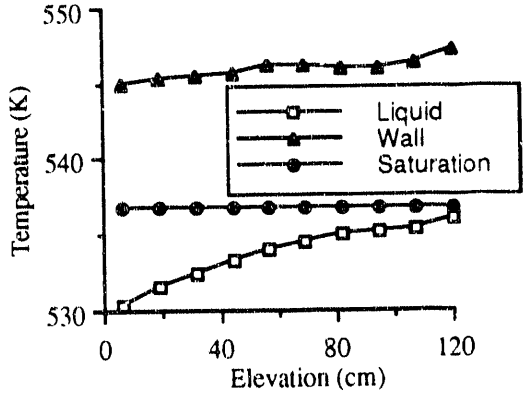

Figure 9. Liquid, Saturation, and Wall Temperatures for the DISCON Simulation at Cycle 500 of the St. Pierre Experiment Run 10.

END

DATE
FILMED
9/22/92